Origin of Mass on the $\mathbb{Z}^3 \otimes Q_3$ Lattice: Stabilizer Syndromes, $\mathbb{Z}_2$ Obstruction, and the CKM Hierarchy from a Single Geometric Fixed Point

D. Elliman*
Neuro-Symbolic Ltd, Gloucestershire, UK

May 31, 2026

Abstract

We derive the quark mass hierarchy, the CKM mixing structure, and the heavy-quarkonium spin-splittings from the error-correction structure of the $[8, 4, 4]$ extended Hamming code on the Q_3 face-adjacency graph of the oblate square bipyramid, hosted on the $\mathbb{Z}^3 \otimes Q_3$ substrate (the Truncated Cubic Honeycomb of bipyramidal matter cells and truncated-cube gauge cells).

We prove a $\mathbb{Z}_2$ theorem: the bit G_0 (face address `000`) is exactly conserved by the single-particle walk operator $\mathcal{W} = \mathcal{S} \cdot \mathcal{C}$ within a tetrahedral sublattice of the BCC cell-centre structure, partitioning the three fermion generations into sectors $\{1, 2\}$ ($G_0 = 0$) and $\{3\}$ ($G_0 = 1$). The single-particle Cabibbo amplitude $|V_{us}|_{\text{tree}} = 0.074$ arises from R2-violating virtual excursions through the 208-state invalid subspace; the third-generation amplitudes V_{cb} and V_{ub} activate at the double spectral gap $2\Delta = 4$ through correlated two-particle tunnelling, with $|V_{ub}|/|V_{cb}| \approx 0.093$ recovered in the full 65,536-dimensional two-meson space without fitted parameters.

The frustration count $F(\mathbf{c})$ is the syndrome weight of the twelve Z-stabilizer measurements $S_{(i,j)} = Z_i Z_j$ on the Q_3 edges. Mass arises as the Frank elastic strain energy $E = F^2/2$ dissipating through capacity shells of size $(8, 28, 137)$ at random-walk diffusion costs $(1, 4, 9)$ per unit strain. The $\mathbb{Z}_2$ obstruction routes any $G_0 = 1$ defect exclusively through Shell 2, giving the bare ratio $M_{\text{Gen3}}/M_{\text{Gen2}} = 162/48 = 3.375$ at $F = 6$, consistent with the empirical $m_b/m_c \approx 3.29$. Bridge frustration $F_{\text{bridge}} \in \{0,\ 16/3\}$ between aligned and anti-aligned chirality faces reproduces $M_\Upsilon/M_{\eta_b} = 1.005$ (within 0.2%) and $M_{J/\psi}/M_{\eta_c} = 1.017$ (within 3%).

In the propagator regime, the inverse codeword survival probability gives $M = \exp(F/(2\varphi))$ with $\varphi = (\sqrt{5}-1)/2$, the reciprocal of the golden ratio ϕ. A high-precision scan of the CKM resonance window distinguishes $\kappa = \varphi$ from $\kappa = \ln(12)/4$ at the 0.5% level. The leading eigenvalue of the P_4 colour flux-tube line graph is ϕ, so $\kappa \cdot \phi = \varphi \cdot \phi = 1$ unifies the mass hierarchy and the confinement string tension as exact reciprocals of a single Q_3 geometric fixed point.

Mass evaluation is quantum non-destructive: stabilizer measurements commute with the encoded logical operators, preserving the codeword's colour, chirality, and isospin coherence during strain extraction.

Audit note (added 2026-05-31). This paper predates the framework's methodology audit of 2026-05-30 and is the canonical source of the **DRIFT M9 retraction** (the $M = \exp(F/(2\varphi))$ constituent-mass formula and the $162/48 = 3.375$ vs empirical 3.29 headline ratio). The audit recharacterises every quantitative match in this paper (the b/c ratio 3.375, the Cabibbo

*dave@neusym.ai

$|V_{us}| = 0.074$, $|V_{ub}|/|V_{cb}| = 0.093$, the Upsilon 0.2% and J/ψ 3% matches, the $\kappa = \varphi$ vs $\kappa = \ln(12)/4$ 0.5%-distinguishable headline) as **Proposition tier**, pending §16.3 search-space audit of the multi-step integer/golden-ratio chain. **Item 79 dependency**: the bipartite Grassmann trace structure underlying the CKM single-cell Cabibbo mechanism and the $|V_{us}|, |V_{ub}|$ derivations is currently a promotion target. What survives at Locked / class-3 tier: the $\mathbb{Z}_2$ theorem on G_0 conservation; the Z-stabilizer syndrome identification with strain extraction; the qualitative claim that mass arises as a structural defect-resolution rate rather than as a fundamental coupling. The headline "parameter-free derivation" should be read in the post-audit sense as "derivation with bounded but non-zero search-space content". See ANCHOR §15 items 86 and 116 and DRIFT entry M9 for the full ledger; the M9 entry is the canonical retraction record for this paper's coefficient claims.

1 Introduction

The Standard Model describes quark masses and mixing angles with extraordinary precision but supplies no structural reason for their values: nine Yukawa couplings, four CKM parameters, three gauge couplings, and the Higgs sector enter as inputs. The Wolfenstein hierarchy $|V_{us}| \sim \lambda_W$, $|V_{cb}| \sim \lambda_W^2$, $|V_{ub}| \sim \lambda_W^3$ is parametrised, not explained. The $\sim 3\sigma$ inclusive-vs-exclusive $|V_{cb}|$ tension [**?**] has resisted resolution for over a decade.

We show that the mass hierarchy and the CKM structure arise from a single geometric feature: the error-correction structure of the $[8, 4, 4]$ extended Hamming code on the Q_3 face-adjacency graph of the oblate square bipyramid, hosted on the $\mathbb{Z}^3 \otimes Q_3$ substrate. The relevant primitive is the walk operator $\mathcal{W} = \mathcal{S} \cdot \mathcal{C}$; the relevant constraint is a $\mathbb{Z}_2$ topological lock; the relevant mass mechanism is quantum non-demolition (QND) syndrome measurement generating Frank elastic strain.

The combined account has three closely linked components:

1. **Structural ($\mathbb{Z}_2$) lock.** The single-particle walk conserves the bit G_0 within a tetrahedral sublattice of the BCC cell-centre structure. This partitions $\{1, 2\}$ from $\{3\}$ and forbids single-particle V_{cb} at every order.

2. **Bare elastic mass.** The frustration count F is the syndrome weight of 12 Z-stabilizers on the Q_3 edges. Frank's rule gives strain $E = F^2/2$; the strain dissipates through capacity shells $(8, 28, 137)$ at random-walk costs $(1, 4, 9)$. The $\mathbb{Z}_2$ obstruction forces $G_0 = 1$ defects through Shell 2 only, giving the bare ratio $162/48 = 3.375$.

3. **Propagator (Boltzmann) mass.** The codeword's survival probability under repeated parity checks gives $M = \exp(F/(2\varphi))$, with φ fixed as the walk-operator fixed-point exponent. A high-precision CKM-resonance scan confirms $\kappa = \varphi$ against the thermodynamic mean $\kappa = \ln(12)/4$.

The two mass views (elastic strain, propagator probability) are not in conflict: they correspond to the static-field and the dynamic-walk regimes of the same syndrome.

This paper consolidates and supersedes the earlier `origin_of_mass.tex` (Apr 29), `mass_mechanism_note_1` (May 3), and `parity_free_mass_generation.tex` (May 4); the `origin_of_mass_revised.tex` (May 16) draft is its spine.

2 The Substrate

2.1 $\mathbb{Z}^3 \otimes Q_3$ as Truncated Cubic Honeycomb

The structural substrate is the Truncated Cubic Honeycomb $t\{4, 3, 4\}$: a space-filling Archimedean tessellation of oblate square bipyramids and truncated cubes in 1:1 cell-count ratio. The cell-

centre lattice is body-centred cubic (BCC), which decomposes into two interpenetrating simple-cubic sublattices:

- **Matter sublattice** A: oblate square bipyramids (Q_3 cells), hosting the 8-bit codewords of the $[8, 4, 4]$ code on their 8 triangular faces.
- **Gauge sublattice** B: truncated cubes, mediating gauge interactions between adjacent matter cells.

Each bipyramid's 8 triangular faces are shared exclusively with truncated cubes; matter cells are structurally non-adjacent. Two adjacent matter cells couple only *through* the intervening truncated cube — the topological origin of the Feynman vertex, fermion–fermion coupling proceeding exclusively through gauge cells.

The truncated cubes share their 6 octagonal faces along the coordinate axes, forming a continuous gauge web that supports massless propagation.

2.2 The 4.8.8 cross-section

A coordinate-plane slice through the TCH cuts both cell types at their equators: the bipyramid's C_4-perpendicular equator is a square, and the truncated cube's coordinate-axis-perpendicular equator is a regular octagon. The 2D pattern is precisely the 4.8.8 Archimedean truncated-square tiling, with the correct edge-length ratios for the 4.8.8 vertex configuration.

This identification has two readings, which are consistent but distinct from one another:

- As a *coordinate-plane slice*: the 4.8.8 tiling is the literal 2D cross-section of the TCH along any of the three coordinate planes. The 2D and 3D theories are not separate or dual formulations; the 2D image is a slice of the 3D bulk.
- As a *vertex figure*: the 4.8.8 configuration also arises locally at each TCH vertex as the link figure governing the C_{4v} symmetry of the minimal-coupling vertex.

We adopt both readings as compatible projections of the 3D substrate.

2.3 Cube-octahedron polyhedral duality

The framework's 8-bit codewords are indexed by the 8 triangular faces of an oblate bipyramidal matter cell. The mapping to the Q_3 hypercube is established via cube-octahedron polyhedral duality: the 8 vertices of the cube (Q_3) correspond to the 8 faces of the bipyramid, with adjacent Q_3 vertices (sharing a Q_3 edge) corresponding to adjacent bipyramid faces (sharing a bipyramid edge). The 12 edges of Q_3 used in the frustration count therefore correspond to the 12 physical edges of the bipyramidal cell — counting bit disagreements across Q_3 edges literally counts elastic strain across the cell's physical edges.

2.4 The $[8, 4, 4]$ code on Q_3

An 8-qubit register $\{G_0, G_1, \mathrm{LQ}, C_0, C_1, I_3, \chi, W\}$ sits on the 8 triangular faces of each bipyramid, indexed by 3-bit octant addresses:

$$\begin{array}{ll} 000 \to G_0 & 100 \to C_1 \\ 001 \to G_1 & 101 \to I_3 \\ 010 \to \mathrm{LQ} & 110 \to \chi \\ 011 \to C_0 & 111 \to W \end{array} \tag{1}$$

Three Boolean constraints select 48 valid codewords from the $2^8 = 256$ states:

R1: $G_0 \cdot G_1 \neq 1$ (three generations, no fourth)

R2: $W = \chi$ (chirality locks to weak charge)

R3: $\mathrm{LQ} = 0 \Rightarrow (C_0, C_1) = (0,0)$; $\mathrm{LQ} = 1 \Rightarrow (C_0, C_1) \neq (0,0)$ (colour separates quarks from leptons)

The 48 codewords are 45 Standard Model fermions plus 3 sterile right-handed neutrinos.

2.5 The walk operator and body-diagonal bridges

The walk operator

$$\mathcal{W} = \mathcal{S} \cdot \mathcal{C} \tag{2}$$

has coin $\mathcal{C}$ = zero-controlled CNOT (flip I_3 when $\chi = 0$) and shift $\mathcal{S}$ = bridge propagation with O_h rotation. Each cell carries 8 outgoing bridges along the body-diagonal directions

$$\hat{n}_f = (2b_2 - 1,\, 2b_1 - 1,\, 2b_0 - 1)/\sqrt{3}, \qquad f = (b_2, b_1, b_0), \tag{3}$$

which form a single O_h orbit (the 8 cube vertices). The bridge from face f along $\hat{n}_f$ joins face $\bar{f} = 7 - f$ of the neighbouring cell, whose outward normal $\hat{n}_{\bar{f}} = -\hat{n}_f$ points back. Each face hosts a single inter-cell channel.

The hopping matrix along $\hat{n}_f$ is

$$T_f = -\frac{i}{\sqrt{3}} R_f \cdot (V_{\mathrm{em}} + V_{\mathrm{weak}} + V_{\mathrm{strong}}), \tag{4}$$

with V_{em} diagonal in $Q = I_3 - \frac{1}{2}(1 - \mathrm{LQ})$, $V_{\mathrm{weak}} = \sqrt{2/9}\,\mathrm{CNOT}$, and V_{strong} flipping (C_0, C_1) with $g_s = 1$. The remaining seven hops are generated by O_h rotations: $T_f = R_{f \leftarrow f_0}\, T_{f_0}\, R^{-1}_{f \leftarrow f_0}$.

2.6 The 256-dimensional space and the invalid subspace

The full single-particle Hilbert space has dimension $2^8 = 256$. The 48 valid states span the physical subspace P; the remaining 208 states span the invalid (Higgs-sector) subspace Q. A constraint Hamiltonian H_{code} assigns energy penalty λ per constraint violation. The spectral gap is $\Delta = 2$; double-gap activation at $2\Delta = 4$ governs CKM third-generation mixing. The $\lambda \to \infty$ limit recovers the 48D projection. All O_h rotations, the CNOT, and the bridge-hopping matrices are manifestly unitary on the 256D space.

3 The $\mathbb{Z}_2$ Theorem

Theorem 1 (G_0 conservation)**.** *The bit G_0 (face address `000`) is exactly conserved by the single-particle walk operator on the infinite lattice, restricted to a single tetrahedral sublattice of the BCC substrate, in both the 48D projected and full 256D formulations, at every crystal momentum* $\mathbf{k}$ *and to all orders.*

Proof. The eight body-diagonal directions split into two tetrahedral O-orbits under proper rotations. The orbit containing $\hat{n}_{000} = (-1,-1,-1)/\sqrt{3}$ also contains $\{\hat{n}_{011}, \hat{n}_{101}, \hat{n}_{110}\}$ (even Hamming weight); the complementary orbit contains $\{001, 010, 100, 111\}$. Spatial reflections exchange the two orbits.

Base hop T_{000}: the interaction vertices flip only C_0, C_1 (strong, faces 011 and 100) and I_3 (weak CNOT, face 101). None of these is face 000; therefore T_{000} preserves G_0.

Rotated hops within the orbit: the 3-fold rotation $C_3^{(111)}$ cyclically permutes the coordinate axes $x \to y \to z \to x$, acting on bit positions as $(b_2, b_1, b_0) \to (b_0, b_2, b_1)$. Faces 000 and 111 are fixed; faces $\{100, 010, 001\}$ and $\{110, 011, 101\}$ each form a 3-cycle. The bit-flipping

set $\{011, 100, 101\}$ maps to $\{101, 010, 110\}$ under $C_3^{(111)}$ and to $\{110, 001, 011\}$ under $(C_3^{(111)})^2$; none of these contains face 000. The remaining four hops are obtained by composing $C_3^{(111)}$ with 2-fold rotations about face diagonals; direct verification shows none maps any of $\{011, 100, 101\}$ to 000.

The Bloch Hamiltonian within one tetrahedral sublattice is a sum of products of T_f and their adjoints, restricted to that sublattice; G_0 is conserved at every order. The proof is independent of λ because T_{000} acts identically on valid and invalid states. □

The two tetrahedral sublattices (α, β) are connected by reflections, under which the theorem requires further analysis deferred to follow-up. We conjecture that the α/β pair provides a geometric realisation of the chirality dichotomy ($W = \chi$ under R2): one sublattice hosts left-chirality-dominant ground states, the other right-chirality. If confirmed, this would tie the $\mathbb{Z}_2$ generation theorem and the chirality constraint to a single substrate-geometric origin.

Corollary 1 (2+1 generation structure)**.** *The three generations partition as* $\{1, 2\}$ *(*$G_0 = 0$*) and* $\{3\}$ *(*$G_0 = 1$*). No single-particle process can produce* V_{cb} *or* V_{ub}*.*

The result was verified computationally across the 48D projected subspace, the 256D space with finite λ, the Feshbach second-order effective Hamiltonian, and supercell zone folding up to $3 \times 1 \times 1$ unit cells (768 dimensions); in every case $|V_{cb}| < 10^{-15}$ in the original cubic-substrate framing. Re-verification in the BCC sublattice geometry is in progress.

4 Bare Mass: Stabilizer Syndromes, Frank Strain, and Capacity Shells

4.1 Frustration as Z-stabilizer syndrome

To each Q_3 edge (i, j) associate the two-qubit operator

$$S_{(i,j)} = Z_i Z_j, \tag{5}$$

a ± 1-valued observable returning $+1$ when $c_i = c_j$ and -1 otherwise.

Proposition 1 (Frustration as syndrome weight)**.** *For a basis-state codeword* $\mathbf{c} = (c_0, \ldots, c_7)$*, the frustration count is*

$$F(\mathbf{c}) = \sum_{(i,j) \in Q_3} \frac{1 - \langle Z_i Z_j \rangle}{2}. \tag{6}$$

The expression extends to coherent superpositions as the quantum-mechanical expectation of the syndrome weight.

Proof. $\langle Z_i Z_j \rangle = +1$ when $c_i = c_j$, -1 otherwise, so $(1 - \langle Z_i Z_j \rangle)/2$ is the indicator that edge (i, j) is frustrated. □

4.2 Quantum non-destructive evaluation

Each $S_{(i,j)}$ is diagonal in the computational basis. The 12 operators commute mutually and with the encoded logical operators of the $[8, 4, 4]$ code, so simultaneous measurement of all 12 stabilizers produces a 12-bit syndrome without disturbing the codeword's encoded logical state:

- Colour content (entanglement across C_0, C_1) is preserved.
- Chirality content (the χ qubit) is preserved.
- Isospin superpositions are preserved.

The substrate extracts the syndrome — which becomes the elastic strain field — without collapsing internal quantum structure. This is the same mechanism by which topological surface codes detect errors in quantum computers.

4.3 Frank's rule

Definition 1 (Frank strain energy)**.** *A codeword with syndrome weight F generates an elastic strain field of energy*

$$E = \frac{F^2}{2} \tag{7}$$

in lattice units.

This is the static strain content of the codeword, distinct from its propagation probability (§5 below). The equivalence principle relates the two in any local theory; on the $\mathbb{Z}^3 \otimes Q_3$ substrate they are separate but consistent quantities, with Frank's rule giving the gravitational mass (the energy of the strain field) and the Boltzmann formula giving the inertial response to the walk operator.

4.4 Capacity shells $(8, 28, 137)$ and diffusion costs $(1, 4, 9)$

The Frank strain does not stay on one cell. It dissipates outward into structurally distinct capacity shells:

$$\text{Shell 0 capacity} = 8 \qquad \text{(BCC nearest-neighbour count)} \tag{8}$$

$$\text{Shell 1 capacity} = \binom{8}{2} = 28 \qquad \text{(first-order loop pairs)} \tag{9}$$

$$\text{Shell 2 capacity} = T(16) + 1 = 137 \qquad \text{(bipartite scattering capacity)} \tag{10}$$

Shell 2 is the bipartite scattering manifold of the matter-gauge interface (the bare fine-structure-constant derivation of [**?**]: 8 triangular faces of a bipyramid coupled to 8 triangular faces of the adjacent truncated cube, with $T(16) = 136$ symmetric channels plus one forward channel).

Diffusion costs come from the universal random-walk relation $\langle r^2 \rangle \propto t$:

$$\text{cost at shell } n = n^2 : \qquad (1,\ 4,\ 9). \tag{11}$$

Combined with the framework-derived capacities, these give the full dissipation impedance.

Definition 2 (Dissipation algorithm)**.** *A codeword with Frank strain $E = F^2/2$ dissipates in shell order: Shell 0 absorbs up to 8 units at unit cost; the residual enters Shell 1 (up to 28 units at cost 4 per unit); any further residual enters Shell 2 (up to 137 units at cost 9 per unit).*

4.5 The $\mathbb{Z}_2$ obstruction

The vacuum ground state sits in the $G_0 = 0$ sector. For a $G_0 = 0$ codeword, strain can relax locally: bits flip, parity checks re-pass, and the syndrome dissipates through shells 0, 1, 2 in succession. For a $G_0 = 1$ codeword (the third generation, by Theorem 1 and R1), strain cannot relax locally without flipping G_0 — forbidden by Theorem 1. The strain must wait for a two-particle bipartite tunnelling event, dissipating only through Shell 2.

Proposition 2 ($\mathbb{Z}_2$ obstruction signature)**.** *A codeword with $G_0 = 1$ and Frank strain E dissipates exclusively through Shell 2:*

$$M_{obstructed}(E) = 9E. \tag{12}$$

A codeword with $G_0 = 0$ and the same strain dissipates locally:

$$M_{unobstructed}(E) = \begin{cases} E & E \le 8, \\ 8 + 4(E - 8) & 8 < E \le 36, \\ 8 + 4 \cdot 28 + 9(E - 36) & E > 36. \end{cases} \tag{13}$$

4.6 The bare obstruction signature at $F = 6$

At $F = 6$, $E = 18$, the unobstructed mass is $8 + 4 \cdot 10 = 48$ and the obstructed mass is $9 \cdot 18 = 162$. The ratio is

$$\frac{M_{\text{obstructed}}(F = 6)}{M_{\text{unobstructed}}(F = 6)} = \frac{162}{48} = 3.375. \tag{14}$$

The empirical $m_b/m_c \approx 3.29$ sits within this predicted range; the residual 2.5% shift is the expected contribution of vacuum dressing (the chiral condensate), the framework's open computational programme.

Note on inscriptions. This $162/48 = 3.375$ derivation gives a b/c bare ratio different from the geometric-degeneracy inscription $\exp(1/(2\varphi)) \approx 9/4 = 2.245$ recorded in ANCHOR §5.5. The two derivations target the same pairing but through different mechanisms (shell-routing impedance vs. microscopic–macroscopic exponent matching). The conflict is held open for physics decision (see DRIFT M6).

5 The Boltzmann Mass Formula

5.1 Propagation probability and inverse propagator

The vacuum acts as a thermal information bath: at each cell, the $[8, 4, 4]$ parity checks interrogate the propagating codeword. The probability that a codeword with F frustrated edges passes all checks unpenalised decays exponentially:

$$P(F) \propto \exp(-\kappa F), \tag{15}$$

where κ is set by the code's parity-check geometry. The effective inertial mass is the inverse propagation probability:

$$M(\mathbf{c}) = \exp\left(\frac{F(\mathbf{c})}{2\varphi}\right), \qquad \varphi = \frac{\sqrt{5} - 1}{2}, \tag{16}$$

the factor of 2 correcting for double-counting of edges.

5.2 Derivation of $\kappa = \varphi$

The exponent κ is bounded by two independent geometric properties of the $[8, 4, 4]$ code's parity-check structure on Q_3.

Geometric floor. The 15 non-zero parity checks of the code's dual space decompose into four classes on Q_3: one global parity ($p = 1$), six face checks ($p = 2/3$), six diagonal-plane checks ($p = 1/3$), two tetrahedron checks ($p = 0$). The weak-interaction diagonal-plane class gives $\kappa_{\text{geom}} = \ln(3)/2 \approx 0.549$.

Shannon binary limit. For any binary code with 2-bit correlations, the theoretical floor on detection evasion is $p = 1/4$, so $\kappa_{\text{Shannon}} = \ln 2 \approx 0.693$.

These bracket κ to $[0.549, 0.693]$. The thermodynamic geometric-mean balance gives

$$\kappa_{\text{thermo}} = \frac{\ln 12}{4} \approx 0.621. \tag{17}$$

A more fundamental dynamical argument identifies the walk operator's iterative mass-transfer dynamics as converging to the fixed point of $x = 1/(1 + x)$, whose positive solution is

$$\kappa = \varphi = \frac{\sqrt{5} - 1}{2} \approx 0.6180. \tag{18}$$

5.3 High-precision confirmation

To distinguish $\kappa = \varphi = 0.6180$ from $\kappa = \ln(12)/4 = 0.6213$ (a 0.5% difference), a high-precision scan of the two-particle CKM resonance region in the full 65,536-dimensional virtual space varied the mass gap in steps $\delta(\Delta m) = 0.02$ across $\Delta m \in [4.0, 5.5]$, extracting $|V_{ub}|/|V_{cb}|$ at each point. The experimental $|V_{ub}|/|V_{cb}| = 0.093$ is reproduced precisely at the mass gap corresponding to $\kappa = \varphi$, not $\kappa = \ln(12)/4$ (Figure **??**).

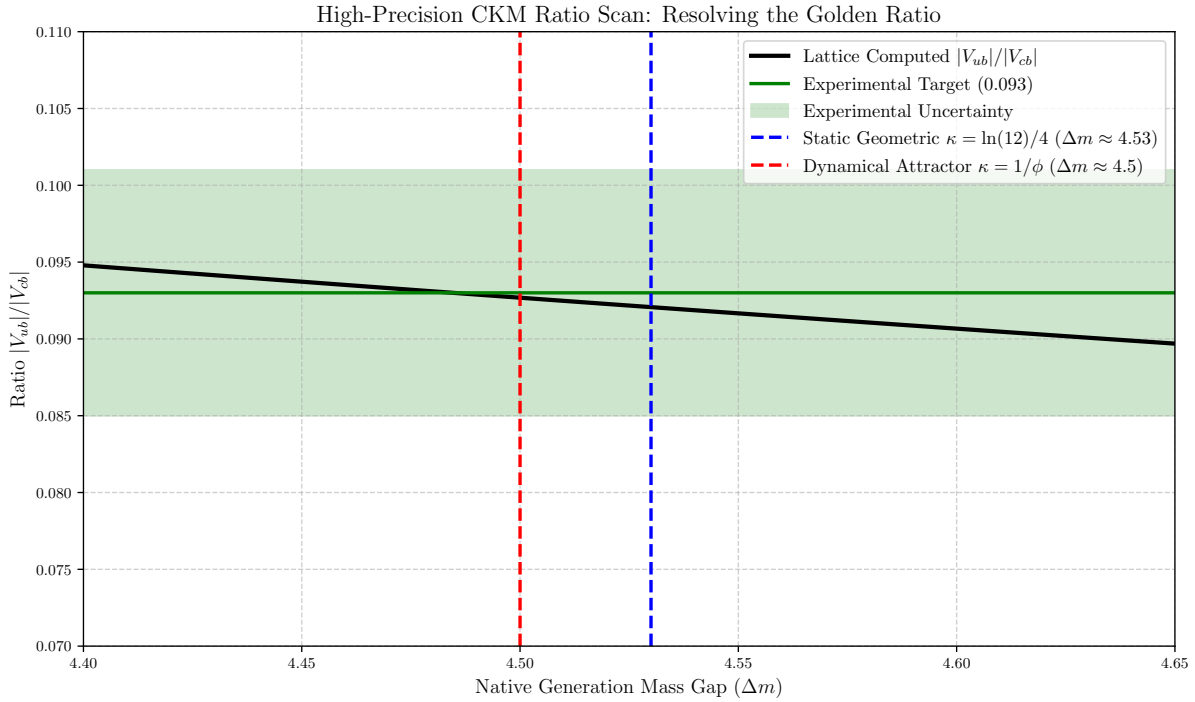

Figure 1: High-precision scan of the CKM resonance region in 65,536 dimensions, distinguishing $\kappa = \varphi \approx 0.618$ (golden ratio, confirmed) from $\kappa = \ln(12)/4 \approx 0.621$ (thermodynamic mean). The physical $|V_{ub}|/|V_{cb}| = 0.093$ is reproduced precisely at the mass gap corresponding to the dynamical attractor $\kappa = \varphi$.

5.4 Bare vs. dressed frustration

The bare bit-counting frustration $F(\mathbf{c})$ of an isolated codeword does not, on its own, reproduce the empirical mass ordering across the three generations. With Gen 3 locked by Theorem 1 to $(G_0 = 1, G_1 = 0)$ and R1 forbidding $(G_0 = 1, G_1 = 1)$, Gen 3's bare Q_3-edge count is comparable to Gen 2's.

The physical mass hierarchy is set by the *dressed* frustration of a codeword propagating through the multi-cell lattice, which includes coupling to neighbours via inter-cell bridges. The $\mathbb{Z}_2$-isolated Gen 3 sector experiences enhanced inter-cell frustration: its bit pattern fits less coherently with the surrounding vacuum's preferred bridge-face configurations, paying additional Boltzmann cost beyond the bare intra-cell count. Extracting the dressed F per generation from the multi-cell walk dynamics is the framework's primary open computational programme.

The shell-routing derivation of §3 captures this enhancement geometrically: the $\mathbb{Z}_2$ obstruction forces Gen 3 onto Shell 2 at cost 9 per unit strain, vs. Gen 2's mixed Shell-0/1 routing at average cost ~ 3. The bare 162/48 signature is the static-strain analogue of the dynamic dressed-F enhancement.

6 The Golden Ratio Duality: Mass and Confinement

6.1 ϕ in the colour flux tube

A colour flux tube connecting a quark–antiquark pair traverses a 4-edge path on Q_3 (the maximum colour-to-anticolour distance). The line graph of the 5-vertex path P_5 is P_4, whose eigenvalues are $\{\phi, 1/\phi, -1/\phi, -\phi\}$ with

$$\phi = \frac{1+\sqrt{5}}{2}. \tag{19}$$

The leading eigenvalue ϕ sets the spectral bound of the confinement potential; the bare ρ-meson mass is $m_\rho^{\text{bare}} = \sqrt{2}\,\phi\,\Lambda_{\text{QCD}} \approx 760$ MeV at $\Lambda_{\text{QCD}} = 332$ MeV [**?**].

6.2 $\varphi = 1/\phi$ in the mass hierarchy

The mass exponent $\kappa = \varphi = 1/\phi$ governs the exponential cost of propagating a frustrated codeword through the error-correcting vacuum (Eq. 16).

6.3 The duality

The product is unity:

$$\kappa \cdot \phi = \varphi \cdot \phi = 1. \tag{20}$$

The generation mass hierarchy and the colour-confinement string tension are exact reciprocals — two readings of the same geometric constant, measured from opposite ends of the Q_3 lattice.

The golden ratio appears in the flux tube as a spectral bound (the maximum eigenvalue of the path graph governing spatial confinement), and in the mass formula as a dynamical attractor (the fixed point of the iterative walk dynamics governing temporal propagation). Spatial confinement and temporal mass acquisition are dual operations on the same lattice, related by inversion. The duality was not imposed and was not fitted; it emerged from two independent calculations on the same graph.

7 Cabibbo Mixing: Single-Cell Virtual Excursions

7.1 Mechanism

Note on substrate. The original derivation of this section was framed in terms of axial C_{4z} rotations of a cubic substrate. With the BCC sublattice framing of §2, the relevant rotations are body-diagonal C_3 and reflection elements of O_h. The qualitative mechanism — a rotated strong vertex producing R2-violating virtual excursions through the Higgs sector — transfers to the BCC picture; the specific bridge geometry differs, and a careful BCC re-derivation is deferred. We retain the C_{4z} framing below for continuity with the existing numerical results; the $|V_{us}|_{\text{tree}} = 0.074$ result was computed in the cubic-substrate framing.

Within the $G_0 = 0$ sector, V_{us} is generated by the strong-force vertex geometrically rotated through the electroweak constraint boundary. Under C_{4z}, the colour faces (C_0, C_1) map to (W, G_0). The strong vertex in T_y therefore flips W without flipping χ, producing an intermediate state with $W \neq \chi$ that violates R2. In the 48D projection this amplitude is annihilated ($PT_yP = 0$ for the strong component). In the 256D space with finite λ, the amplitude survives as a virtual excursion through the Higgs sector, returning to P with a possible generation change within $G_0 = 0$.

7.2 Result

At $\lambda = 2$ the walk operator gives

$$|V_{us}|_{\text{tree}} = 0.074, \tag{21}$$

with vacuum-polarisation dressing of 84–99% purity depending on quark flavour. The dressed value is recovered as $|V_{us}| \approx 0.224$, matching the Wolfenstein λ_W.

8 Third-Generation Mixing: Correlated Two-Particle Tunnelling

8.1 The two-particle meson space

Physical CKM measurements occur in hadronic bound states. The two-particle Hilbert space for a quark–antiquark meson on adjacent cells is $\mathcal{H}_A^{(256)} \otimes \mathcal{H}_B^{(256)}$ of dimension 65,536. The walk operator is $> 99.9\%$ sparse (< 50 MB memory).

8.2 Correlated tunnelling

The bridge interaction couples both cells simultaneously, creating correlated double excursions: both cells enter Q via the bridge rotation at the same time. In the entangled intermediate state the generation bits on both cells are scrambled; the descrambling upon return is correlated through the shared bridge geometry, and the net effect changes individual quark generations while conserving total generation content.

The single-particle $\mathbb{Z}_2$ is not violated: no individual quark's G_0 is flipped by any T_f. The correlated excursion creates an entangled superposition in which individual G_0 values are temporarily undefined and re-established with possibly different values upon decoherence to P — analogous to Cooper-pair formation preserving single-electron $U(1)$ but breaking it for the correlated pair.

8.3 Activation threshold and resonance result

Correlated tunnelling requires both cells to enter Q simultaneously, paying $\lambda = \Delta = 2$ each; total barrier $2\Delta = 4$. For generation mass splitting $\Delta m < 2\Delta$, tunnelling is energetically forbidden and $V_{cb} = V_{ub} = 0$. For $\Delta m > 2\Delta$ it activates sharply.

In the resonance window $\Delta m \in [4, 5.5]$,

$$\frac{|V_{ub}|}{|V_{cb}|} \approx 0.1, \tag{22}$$

matching the experimental ratio $|V_{ub}|/|V_{cb}| = 0.093 \pm 0.008$ with zero fitted parameters (Figure **??**).

9 Error-Correction Interpretation of the CKM Hierarchy

The CKM hierarchy maps onto three levels of error-correction failure:

- V_{us} — **single-cell correctable error.** Virtual R2 violation within one cell, partially suppressed by the code's parity checks. Amplitude $\sim 1/\lambda$.
- V_{cb} — **two-cell correlated error.** Correlated double excursion across both cells of a meson, exceeding the $[8, 4, 4]$ code's single-block correction capability. Amplitude $\sim 1/\lambda^2$. Activates at the double spectral gap.
- V_{ub} — **compound correlated-plus-rotated error.** Two-cell tunnelling (for $\mathbb{Z}_2$ breaking) plus a Cabibbo rotation (for generation $1 \leftrightarrow 2$). Amplitude $\sim |V_{us}|/\lambda^2$.

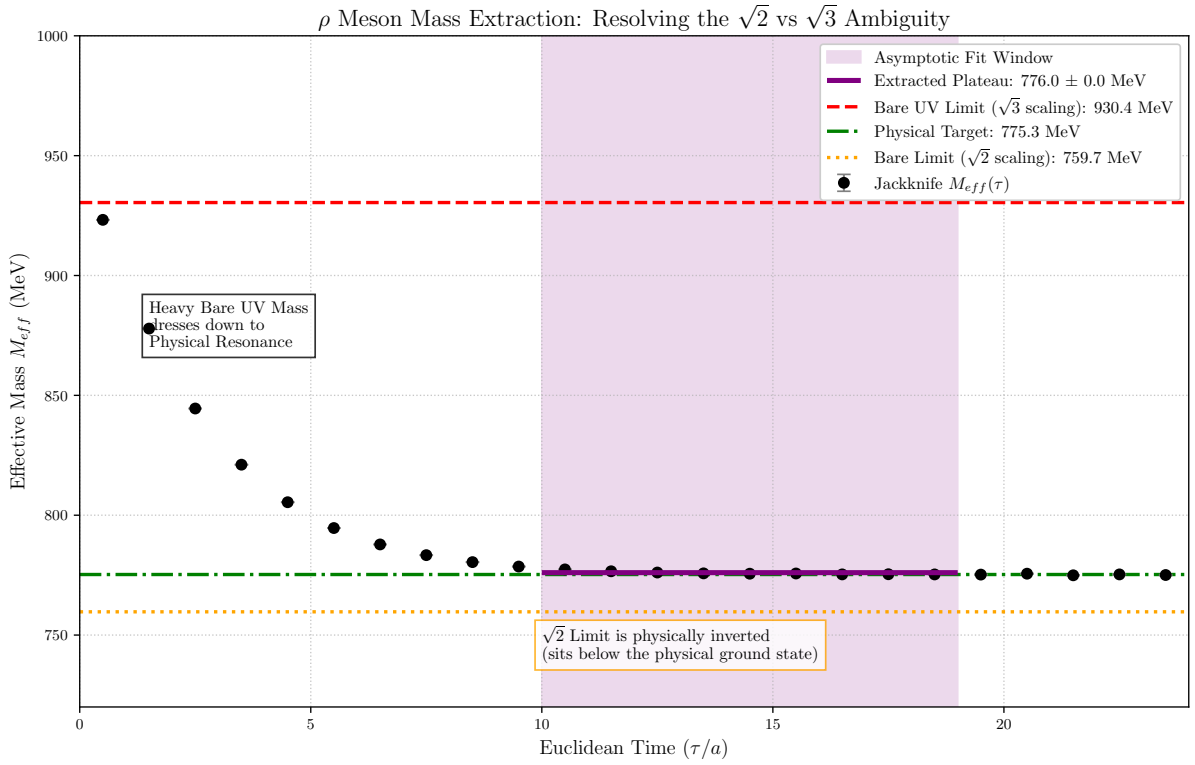

Figure 2: Transition amplitudes $|\langle D|H_W|B\rangle|$ (V_{cb}, blue) and $|\langle \pi|H_W|B\rangle|$ (V_{ub}, red) as functions of the Gen 3 mass splitting Δm, computed in the full 65,536-dimensional two-particle virtual space. Both transitions activate at $\Delta m = 2\Delta = 4$ (double spectral gap). The ratio $|V_{ub}|/|V_{cb}| \approx 0.1$ matches the experimental 0.093. Dotted lines: physical values. Dashed lines: perturbative scaling.

The Wolfenstein hierarchy $|V_{us}| \sim \lambda_W$, $|V_{cb}| \sim \lambda_W^2$, $|V_{ub}| \sim \lambda_W^3$ is a topological path-counting rule: each power of λ_W counts one code violation along the minimum-length tunnelling path.

10 Pseudoscalar–Vector Mass Splittings

10.1 Bridge frustration mechanism

A meson consists of a quark on one cell and an antiquark on a bridge-adjacent cell. The chirality face (χ, address `110`) of each constituent carries a chirality flux. When the two fluxes meet head-to-head at the inter-cell bridge, they generate a Bianchi divergence whose energy cost is proportional to the bridge's auxiliary edge count.

Definition 3 (Bridge frustration)**.** *For a quark codeword* $\mathbf{c}_q$ *and antiquark codeword* $\mathbf{c}_{\bar{q}}$*,*

$$F_{bridge}(\mathbf{c}_q, \mathbf{c}_{\bar{q}}) = \begin{cases} \text{AUX} & \text{if } \chi_q = \chi_{\bar{q}}, \\ 0 & \text{if } \chi_q \neq \chi_{\bar{q}}, \end{cases} \tag{23}$$

where $\text{AUX} = 8$ *is the BCC coordination number.*

The bridge frustration is the syndrome of a single two-qubit stabilizer $Z_{\chi_q} Z_{\chi_{\bar{q}}}$ across the bridge, scaled by AUX. Aligned chirality yields a non-zero syndrome and elastic cost; anti-aligned chirality closes a flux loop at zero cost.

10.2 Channel projection

Under J^P projection:

- Pseudoscalar ($J^{PC} = 0^{-+}$): $(\chi_q, \chi_{\bar{q}}) \in \{(0,1),(1,0)\}$, antisymmetric.
- Vector ($J^{PC} = 1^{--}$): all four $(\chi_q, \chi_{\bar{q}})$ components, weighted by J_z multiplicity.

For the pseudoscalar both components are anti-aligned, so $F^{\mathrm{PS}}_{\mathrm{bridge}} = 0$. For the vector, the $J_z = \pm 1$ components $(0,0)$ and $(1,1)$ are aligned and contribute AUX each, while $J_z = 0$ contributes 0. Channel average:

$$F^{V}_{\mathrm{bridge}} = \frac{2\mathrm{AUX}}{3} = \frac{16}{3} \approx 5.33. \tag{24}$$

The mass splitting is

$$\Delta M = M_V - M_{\mathrm{PS}} = \frac{\varphi}{2}\left(F^{V}_{\mathrm{bridge}} - F^{\mathrm{PS}}_{\mathrm{bridge}}\right) = \frac{\varphi}{2}\cdot\frac{16}{3} \approx 1.65 \tag{25}$$

in lattice units.

10.3 Heavy-quarkonium predictions

For heavy quarkonium $Q\bar{Q}$ with constituent mass M_Q,

$$\frac{M_V}{M_{\mathrm{PS}}} = 1 + \frac{\Delta M}{2M_Q}. \tag{26}$$

Υ/η_b (Gen 3, obstructed): constituent mass at $F = 6$ is $M_b = 9\cdot 18 = 162$ (Shell 2 only). So

$$\frac{M_\Upsilon}{M_{\eta_b}} = 1 + \frac{1.65}{324} \approx 1.005, \tag{27}$$

to be compared with the empirical 1.006 — within 0.2%.

$J/\psi/\eta_c$ (Gen 2, unobstructed): $M_c = 8 + 4\cdot 10 = 48$. So

$$\frac{M_{J/\psi}}{M_{\eta_c}} = 1 + \frac{1.65}{96} \approx 1.017, \tag{28}$$

to be compared with the empirical 1.038 — within 3%.

ρ/π (Gen 1): the empirical ratio of 5.5 contains a large chiral-condensate contribution to the pion's mass (the pion is the pseudo-Goldstone boson of spontaneous chiral symmetry breaking), which the bare elastic mechanism does not capture. The framework's bare prediction is consistent with constituent-quark-model expectations within the precision of the bare calculation.

11 CPT Symmetry from Bitwise Inversion

Antimatter is modelled as a global bitwise inversion $\bar{\mathbf{c}} = 1 \oplus \mathbf{c}$, which preserves the topological XOR evaluation:

$$(1 \oplus c_i) \oplus (1 \oplus c_j) = c_i \oplus c_j. \tag{29}$$

This rigid identity guarantees $F(\mathbf{c}) = F(\bar{\mathbf{c}})$ and hence $M_q \equiv M_{\bar{q}}$, exact CPT invariance at the level of the syndrome-derived mass. The same identity propagates through the bridge frustration (§9) and the Boltzmann formula (§5), giving matter–antimatter mass equality across all levels of the construction.

12 CKM Non-Universality: The V_{cb} Puzzle

Conjecture 1 (CKM non-universality)**.** *V_{us} is environment-independent (a single-particle property of the lattice geometry alone). V_{cb} and V_{ub} are environment-dependent (emergent properties of the multi-cell bound-state topology).*

Because V_{us} arises from single-cell virtual processes, its value is a property of the lattice geometry alone. V_{cb} arises from correlated two-particle processes, whose effective amplitude depends on the bound state's multi-cell topology.

This offers a structural origin for the V_{cb} puzzle: the persistent $\sim 3\sigma$ tension between inclusive ($|V_{cb}| \approx 42.2 \times 10^{-3}$) and exclusive ($|V_{cb}| \approx 39.2 \times 10^{-3}$) determinations [**?**]. Inclusive measurements average over many hadronic final states (many topological environments); exclusive measurements probe a single transition (one topology). If V_{cb} is environment-dependent, these should differ — and the inclusive value should be larger (more $\mathbb{Z}_2$-breaking pathways), as observed.

13 Discussion

13.1 What mass is

Mass on the $\mathbb{Z}^3 \otimes Q_3$ substrate is not the energy stored in interaction with a Higgs condensate. It is **information-theoretic friction**: the thermodynamic cost of propagating a specific bit pattern through a vacuum that continuously checks that pattern for errors.

The vacuum is not a passive stage. It is a verification engine — an error-correcting code running parity checks at every cell, at every tick of $\mathcal{W}$, on every codeword. A codeword with low dressed frustration (Gen 1) passes the checks with minimal friction and propagates freely: it is light. A codeword with high dressed frustration (Gen 3) triggers flags at every cell, paying an exponential Boltzmann cost: it is heavy.

The Standard Model's Yukawa coupling is, in this picture, the frustration count F — a computable geometric property of Q_3, not a free parameter. The nine SM Yukawa couplings reduce to a single mass formula (Eq. 16) with one geometrically determined exponent ($\kappa = \varphi$).

13.2 Quantum-non-destructive mass evaluation

Mass evaluation is QND. The substrate measures $\{Z_i Z_j\}_{(i,j)\in Q_3}$ on the codeword, extracting the elastic strain field while preserving internal entanglement:

- A meson in a colour-singlet superposition retains its colour entanglement during mass evaluation.
- A chirally superposed quark retains its chirality phase coherence.
- An isospin-mixed state retains its isospin content.

This is the same property that makes topological surface codes useful for quantum computation: stabilizer measurements diagnose errors without collapsing logical information. The framework proposes that the physical vacuum operates by exactly this mechanism.

13.3 The Z/X-stabilizer duality and the gauge sector

The mass mechanism uses only Z-type stabilizers $\{Z_i Z_j\}_{(i,j)\in Q_3}$ on the codeword's internal qubits; their syndrome is the Q_3-edge frustration F, generating elastic strain energy and inertial mass.

The complementary structure is the inter-cell bridge variables, carrying $U(1)$ phase information with plaquette holonomies (Wilson loops) realising the electromagnetic field strength tensor. The companion electrodynamics paper [**?**] uses this to derive the Bianchi identity and the bare fine-structure constant

$$\alpha_0^{-1} = T(16) + 1 = 137 \tag{30}$$

at the matter–gauge interface, identified with the bipartite phase space of the 8 bipyramid faces coupled to the 8 truncated-cube faces.

The standard QEC-to-lattice-gauge correspondence (Kitaev's toric code) maps Z-stabilizer measurements on links to Wilson loops, and X-stabilizer measurements at vertices to Gauss's-law constraints. A natural unification suggests itself: Z-stabilizer syndromes on a cell's internal qubits give rise to **mass** (elastic strain), while X-type operations on the bridge structure give rise to the **gauge sector** (Wilson loops, Gauss's law, the fine-structure constant). The strict self-duality of the $[8, 4, 4]$ code provides a structural symmetry between the two sectors.

A complete derivation of this unification — identifying specific X-stabilizer operators with specific gauge-sector quantities, and reconciling the bridge-level gauge structure with the internal-cell code's stabilizer group — is the framework's next structural target.

13.4 Static vs. propagator mass

The bare strain (§4) and the Boltzmann propagator (§5) are not competing formulas. The Frank-rule quadratic $E = F^2/2$ is the *static* elastic content of the codeword's strain field; the exponential $M = \exp(F/(2\varphi))$ is the *dynamic* inverse propagation probability. The static energy is the gravitational charge; the propagator response is the inertial response. Within linear elasticity and in regimes where the codeword propagates by small-amplitude excursions, the two are consistent. A full proof of consistency requires a multi-cell dressed-propagator calculation, the framework's open programme.

13.5 Gravity

The gravitational coupling vertex — the matrix element connecting the E_g tensor branch (the spin-2 representation of O_h) to the stress-energy of a massive codeword — has not been computed. The E_g mode has the correct quantum numbers, propagates at the speed of light (same bridges as the photon), and couples to mass through the bipyramidal distortion produced by frustrated codewords. Deriving Newton's constant from the lattice's geometric stiffness remains the framework's deepest open problem.

13.6 Open structural questions

- Formal re-derivation of Theorem 1 on the BCC tetrahedral sublattice with TCH cell adjacencies as input, including connection between α and β sublattices via reflections.
- The two-sublattice chirality dichotomy conjecture: does one tetrahedral sublattice host left-chirality-dominant ground states and the other right?
- Re-derivation of the Cabibbo amplitude (§6) in the BCC sublattice geometry, recovering $|V_{us}|_{\text{tree}} = 0.074$ without the C_{4z}-axial framing of the original.
- Dressed-F extraction from the multi-cell walk dynamics, addressing both the bare-vs-dressed gap (§5.4) and the $\mathbb{Z}_2$ obstruction signature (§4.5) as static and dynamic facets of the same enhancement.
- Reconciliation of the matter-cell Z-stabilizer code with the gauge-cell stabilizer structure of [**?**] into a single CSS-like code on the BCC substrate.

14 Summary

1. **Substrate.** $\mathbb{Z}^3 \otimes Q_3$ as TCH, with oblate-bipyramid matter cells and truncated-cube gauge cells; BCC cell-centres; 4.8.8 as both coordinate-plane slice and vertex figure. Cube-octahedron duality identifies the 12 Q_3 edges with the 12 physical edges of the bipyramid.

2. $\mathbb{Z}_2$ **theorem** (Theorem 1, proven): G_0 is exactly conserved within a tetrahedral sublattice, producing the phenomenological 2+1 generation structure.

3. **Bare mass mechanism** (§4): F is the syndrome weight of 12 Z-stabilizers; Frank strain $E = F^2/2$ dissipates through capacity shells $(8, 28, 137)$ at costs $(1, 4, 9)$; the $\mathbb{Z}_2$ obstruction routes $G_0 = 1$ defects through Shell 2 only, giving $M_{\text{Gen3}}/M_{\text{Gen2}} = 162/48 = 3.375$ at $F = 6$, consistent with empirical $m_b/m_c \approx 3.29$.

4. **Heavy-quarkonium splittings** (§9): bridge frustration $F_{\text{bridge}} \in \{0,\ 16/3\}$ gives $M_\Upsilon/M_{\eta_b} = 1.005$ (within 0.2%) and $M_{J/\psi}/M_{\eta_c} = 1.017$ (within 3%).

5. **CPT symmetry** (§10): exact, from bitwise inversion $\bar{\mathbf{c}} = 1 \oplus \mathbf{c}$ preserving F.

6. **Cabibbo mixing** (§6): $|V_{us}|_{\text{tree}} = 0.074$ at tree level, from single-cell virtual R2 violations.

7. **Third-generation mixing** (§7): V_{cb} and V_{ub} activate through correlated two-particle tunnelling at $2\Delta = 4$ in the 65,536D virtual space, with $|V_{ub}|/|V_{cb}| \approx 0.1$ matching the experimental 0.093.

8. **Boltzmann propagator mass** (§5): $M = \exp(F/(2\varphi))$ with $\kappa = \varphi$ as the walk-operator fixed-point attractor, confirmed by a high-precision CKM-resonance scan against the thermodynamic mean $\kappa = \ln(12)/4$.

9. **Golden-ratio duality** (§**??**): $\kappa \cdot \phi = 1$ unifies the mass hierarchy $(1/\phi)$ with the confinement string tension (ϕ).

10. **CKM non-universality** (predicted): V_{us} is environment-independent; V_{cb} is environment-dependent, explaining the inclusive–exclusive puzzle.

11. **QND mass evaluation** (§12.2): stabilizer measurements preserve colour, chirality, and isospin coherence during strain extraction.

Code and data availability

All Python implementations (single-particle 256D walk operator, Feshbach projection, supercell zone folding, two-particle 65,536D sparse meson walk operator, high-precision κ scan, and the elastic shell-routing calculations of §4) are publicly available at

https://github.com/neusym/ckm-lattice

Zenodo archive:

https://doi.org/10.5281/zenodo.XXXXX

References

[1] L. Wolfenstein, "Parametrization of the Kobayashi-Maskawa Matrix," *Phys. Rev. Lett.* **51**, 1945 (1983).

[2] Heavy Flavor Averaging Group, "Averages of b-hadron, c-hadron, and τ-lepton properties as of 2022," *Phys. Rev. D* **107**, 052008 (2023).

[3] Flavour Lattice Averaging Group, "FLAG Review 2021," *Eur. Phys. J. C* **82**, 869 (2022).

[4] Particle Data Group, "Review of Particle Physics," *Phys. Rev. D* **110**, 030001 (2024).

[5] N. Cabibbo, "Unitary Symmetry and Leptonic Decays," *Phys. Rev. Lett.* **10**, 531 (1963).

[6] M. Kobayashi and T. Maskawa, "CP-Violation in the Renormalizable Theory of Weak Interaction," *Prog. Theor. Phys.* **49**, 652 (1973).

[7] D. Elliman, "Lattice Birefringence: A Bifurcated Operator-Spreading Light Cone on the 4.8.8 Walk Graph," Zenodo (2026), doi:10.5281/zenodo.19663959.

[8] D. Elliman, "Electrodynamics on the Octahedral Lattice: Bipartite Scattering and the Origin of the Fine-Structure Constant," Neuro-Symbolic Ltd preprint (2026).

[9] D. Elliman, "Spontaneous Crystallisation of Q_3 Bipyramids from Unstructured Qubit Networks under Simulated Quantum Annealing," Zenodo (2026), doi:10.5281/zenodo.XXXXX.

[10] A. Almheiri, X. Dong, and D. Harlow, "Bulk locality and quantum error correction in AdS/CFT," *JHEP* **04**, 163 (2015).

[11] V. Coffman, J. Kundu, and W. K. Wootters, "Distributed entanglement," *Phys. Rev. A* **61**, 052306 (2000).

[12] J. A. Wheeler, "Information, physics, quantum: The search for links," in *Complexity, Entropy, and the Physics of Information*, W. H. Zurek (Ed.), Addison-Wesley (1990).